CDDpress

www.nature.com/cdd

ARTICLE

Check for updates

The deubiquitylating enzyme USP35 restricts regulated cell death to promote survival of renal clear cell carcinoma

Shanshan Wang[1,5], Taishu Wang[1,2,5], Xuehong Zhang[1], Shaoxuan Cheng[1], Chaoqun Chen[1], Guoheng Yang[1], Fuqiang Wang[1], Ruilin Wang[1], Qingqing Zhang[3], Dian Yang[1], Yingqiu Zhang[1], Shuyan Liu[1], Hongqiang Qin[4], Quentin Liu[1] and Han Liu[1]✉

The ubiquitin-proteasome system governs a wide spectrum of cellular events and offers therapeutic opportunities for pharmacological intervention in cancer treatment. Renal clear cell carcinoma represents the predominant histological subtype and accounts for the majority of cancer death related to kidney malignancies. Through a systematic survey in the association of human ubiquitin-specific proteases with patient prognosis of renal clear cell carcinoma and subsequent phenotypic validation, we uncovered the tumor-promoting role of USP35. Biochemical characterizations confirmed the stabilizing effects of USP35 towards multiple members of the IAP family in an enzymatic activity-dependent manner. USP35 silencing led to reduced expression levels of IAP proteins, which were accompanied with increased cellular apoptosis. Further transcriptomic analysis revealed that USP35 knockdown affected the expression levels of NRF2 downstream transcripts, which were conferred by compromised NRF2 abundance. USP35 functions to maintain NRF2 levels by catalyzing its deubiquitylation and thus antagonizing degradation. NRF2 reduction imposed by USP35 silencing rendered renal clear cell carcinoma cells increased sensitivity to ferroptosis induction. Finally, induced USP35 knockdown markedly attenuated xenograft formation of renal clear cell carcinoma in nude mice. Hence, our findings reveal a number of USP35 substrates and uncover the protecting roles of USP35 against both apoptosis and ferroptosis in renal clear cell carcinoma.

Cell Death & Differentiation (2023) 30:1757–1770; https://doi.org/10.1038/s41418-023-01176-3

INTRODUCTION

Kidney cancer is a frequently diagnosed malignancy affecting the urinary system, with over 430,000 new cases reported annually worldwide [1]. Renal clear cell carcinoma (RCC) represents the predominant histological subtype that accounts for about 75% of all cases, followed by papillary type and chromophobe that comprise up to about 15% and 5%, respectively [2]. RCC also accounts for the majority of kidney cancer-related deaths and therefore remains as the focus of clinical investigation. Recent progresses have established the kinase inhibitors such as sorafenib and sunitinib, as well as the immune checkpoint antibodies exemplified by nivolumab and pembrolizumab as effective therapies in the treatment of RCC [3].

The ubiquitin-proteasome system plays pivotal roles in many aspects of cellular physiology, and therefore has been proposed as a valuable source for drug target identification and development [4, 5]. Recent analysis of multi-omics data has also revealed that approximately 20% of cancer driver genes are associated with dysregulated functions relating to protein degradation in the ubiquitin-proteasome system [6]. Intriguingly, alterations in selective protein degradation is closely linked to the tumorigenesis of RCC, given that a dominant proportion carries mutation of the *VHL* gene, which encodes an adaptor subunit of the cullin E3 ubiquitin ligase complex mediating the degradation of the hypoxia-inducible factor (HIF) [7–9]. These observations suggest the great potential of investigation and exploitation of the ubiquitin-proteasome system to develop novel therapeutic modalities in the treatment of kidney cancer.

Human deubiquitylating enzymes (DUBs) are a group of isopeptidases that function as essential regulators in the ubiquitin-proteasome system primarily through catalyzing the removal of ubiquitin entities off substrate proteins to counteract ubiquitylation-mediated cellular functions [10]. There is emerging evidence linking several deubiquitylating enzymes to the development and progression of renal carcinoma. The BRCA1 associated protein-1 (BAP1), a deubiquitylating enzyme from the ubiquitin C-terminal hydrolase (UCH) subfamily of DUBs, has been disclosed as an important tumor suppressor to curb tumorigenesis of RCC [11, 12]. In addition, USP37 was revealed to promote kidney tumorigenesis and metastasis through stabilizing the protein levels of HIF2α [13]. Despite recent advances, the implications of DUBs in the tumorigenesis of RCC remain incompletely understood.

Ubiquitin-specific protease (USP) is the largest subfamily of human DUBs, comprised of over 50 cysteine proteases [14]. USPs have been closely implicated in the tumorigenesis of malignancies and are proposed as promising therapeutic targets for cancer treatment [15]. In this study, we focus on the involvement of USPs

[1]Institute of Cancer Stem Cell, Dalian Medical University, Dalian, China. [2]National Institute of Biological Sciences, Beijing, China. [3]Department of Pathology, Dalian Medical University, Dalian, China. [4]CAS Key Laboratory of Separation Science for Analytical Chemistry, Dalian Institute of Chemical Physics, Chinese Academy of Sciences, Dalian, China. [5]These authors contributed equally: Shanshan Wang, Taishu Wang. ✉email: liuhan@dmu.edu.cn

Received: 5 February 2022 Revised: 26 April 2023 Accepted: 3 May 2023
Published online: 12 May 2023

in RCC and report USP35 as a critical factor to preclude regulated cell death including apoptosis and ferroptosis. Such multifaceted functions of USP35 are conferred by its capability to deubiquitylate and stabilize various substrate proteins, i.e. the anti-apoptotic inhibitor of apoptosis (IAP) proteins and the redox regulator NF-E2-related factor 2 (NRF2) that antagonize apoptosis and ferroptosis, respectively. As a result, USP35 inhibition compromises the survival of RCC cells by increasing regulated cell deaths and thus represents a vulnerability that offers therapeutic potential.

MATERIAL AND METHODS

Cell culture

RCC 786-O and human embryonic kidney HEK293T cells were purchased from the American Type Culture Collection (ATCC). RCC 769-P cells were obtained from Procell (Wuhan, China), and OS-RC-2 cells were purchased from KeyGEN BioTECH. HEK293T cells were grown with Dulbecco's modified Eagle's medium (DMEM, Gibco) supplemented with 10% foetal bovine serum (Biological Industries) and 1% penicillin/streptomycin (Thermo Fisher Scientific). All RCC cell lines were cultured in RPMI 1640 medium (Gibco), with the addition of 10% foetal bovine serum and 1% penicillin/streptomycin. The plates used for cell culture were purchased from Jet Bio-Filtration Co, Ltd (Guangzhou, China). All cells were routinely tested for mycoplasma contamination and maintained in a humidified cell incubator (Thermo, 3111) at 37 °C containing 5% of CO_2.

Antibodies and reagents

Rabbit anti-USP35 (A302-290A) antibody was purchased from Bethyl. Rabbit anti-c-IAP1 (D5G9), anti-c-IAP2 (58C7), anti-Survivin (71G4B7), anti-XIAP (3B6) and anti-Livin (D61D1) antibodies were purchased from Cell Signaling Technology. Rabbit anti-NRF2 antibody (16396-1-AP) and mouse anti-β-actin antibody were purchased from Proteintech. Mouse anti-Flag (F1804) and anti-α-tubulin (T5168) antibodies were obtained from Sigma. Rabbit anti-GFP antibody (ab6556) was purchased from Abcam. Mouse anti-HA (MMS-101P) and anti-Ubiquitin (P4G7) antibodies were obtained from Covance. Infrared-labeled secondary antibodies (goat anti-rabbit and anti-mouse) for Western blotting were obtained from LI-COR. RSL3, Z-VAD-fmk and ferrostatin-1 were obtained from MedChem Express (Shanghai, China). All chemicals were dissolved as per the manufacturers' instructions.

Cell lysis and Western blotting

For Western blotting, cells were lysed in RIPA lysis buffer (10 mM Tris-HCl pH 7.4, 100 mM NaCl, 1% Nonidet P-40, 50 mM NaF, 1% sodium deoxycholate, and 0.1% SDS) supplemented with phosphatase inhibitor cocktail (Roche) and protease inhibitor cocktail (Sigma) as described previously [16]. Cell lysates were cleared by centrifugation (15,000 × *g*, 4 °C, 15 min). The protein concentrations from lysates were measured using a BCA assay kit (Pierce). Equal amounts of lysate proteins were resolved on 8% SDS-polyacrylamide gel electrophoresis (SDS-PAGE) and transferred to a nitrocellulose membrane. Membranes were blocked in 4% of skimmed milk in PBS for 1 h at room temperature. Afterwards, membrane was incubated with diluted primary antibodies overnight at 4 °C, followed by PBS washes and further incubation with infrared-labeled secondary antibodies at room temperature for 1 h. Finally, images were taken on a LI-COR Odyssey imager and protein band intensities were calculated using Image Studio programme (version 4.0).

Flow cytometry

Apoptosis assay was carried out using propidium iodide (PI) and FITC-Annexin V Apoptosis detection kit (KeyGEN Biotech, China). Briefly, RCC cells were grown in 6-well plates and treated with indicated drugs. After treatment, cells were washed twice using PBS and then detached using trypsin without EDTA for 5 min at 37 °C. Subsequently, 5 × 10^5 cells were resuspended in binding buffer, and incubated with Annexin V-FITC and PI for 15 min in the dark. Finally, samples were analyzed by ACCURI C6 flow cytometer (BD Bioscience, USA). Reactive oxygen species (ROS) levels were measured using the ROS assay kit (Beyotime, China). Briefly, cells cultured in 6-well plates were treated with corresponding drugs for indicated times. Cells were washed using PBS prior to incubation with 10 μM of DCFH-DA for 30 min at 37 °C. Subsequently, cells were trypsinized and resuspended in ice-cold PBS in the dark, before subjected to flow cytometry analysis using an ACCURI C6 flow cytometer. Acquired data were analyzed using the FlowJo software (version 10).

Cell death detection with PI staining

A total of 3 × 10^5 renal cancer cells were seeded into each well of a 6-well plate that was maintained in the cell incubator. Next day, cells were treated with indicated drugs for required times. After treatment, cells were stained with PI (1 μg/ml final concentration) for 10 min at 37 °C. Then cells were immediately examined under a fluorescence microscope equipped with a 10× phase contrast objective (Olympus IX81, Japan). Phase contrast and fluorescence images were captured, with dead cells indicated by positive PI staining analyzed using the ImageJ software.

Immunoprecipitation assay

Immunoprecipitation was carried out as described previously [17]. In brief, cells were washed using ice-cold PBS and lysed with the Triton X-100 lysis buffer (50 mM Tris-HCl pH7.4, 150 mM NaCl, 1 mM EDTA, 1% Triton X-100, 2 mM Na_3VO_4, 1 mM PMSF). For experiments to detect ubiquitylation signals, the cysteine peptidase inhibitor N-ethylmaleimide (NEM, Sigma) was added to a final concentration of 10 mM in the lysis buffer. Cell lysates were centrifuged at 15,000 × *g* at 4 °C for 15 min. After protein concentration determination, equal amounts (0.5–1 mg) were incubated with target antibody and protein G sepharose (Roche), which were then mixed on a rotator for 2 h at 4 °C. After incubation, samples were washed 4 times with the IP wash buffer (50 mM Tris-HCl pH 7.4, 150 mM NaCl, 0.1% Triton X-100). Immunoprecipitation samples were finally eluted using 1.5 × SDS-PAGE loading buffer and analyzed by Western blotting.

MTT assay

Cell proliferation was estimated by performing MTT assays. Cultured renal cancer cells were counted and seeded into 96-well plate (5000 cells per well), followed by incubation with corresponding drugs for indicated times. After treatment, 3-(4, 5-dimethylthiazol-2-yl)-2, 5-diphenyltetrazolium bromide (MTT) was added to cells that were incubated at 37 °C for 3 h. Subsequently, DMSO was added into each well to dissolve formazan from reaction. Plates were mixed thoroughly and finally absorbance at 570 nm and 630 nm was recorded using a spectrometer (Perkin Elmer).

Colony formation assay

Cultured renal 786-O, OS-RC-2 and 769-P cells were harvested and pipetted to become single-cell suspension before plated with the same numbers into 6-well plates (1000 cells per well). Cells were incubated at 37 °C in the cell incubator for 10 days, with medium refreshed every three days. Cell colonies were fixed in ice-cold methanol for 10 min and visualized by staining with 0.1% of crystal violet as described [18]. The colonies were rinsed several times with PBS, and images were acquired using a Bio-Rad imaging System. The numbers of colonies were quantified using the ImageJ software.

Plasmids, shRNAs and lentivirus preparation

Full-length *USP35 wild-type*, *USP35 C450A*, *BIRC2*, *BIRC3*, *BIRC4*, *BIRC5*, *BIRC7*, *BIRC8* and *NFE2L2* (NRF2) were cloned into the pCMV-3xFlag, pEGFP-C1 and pCDNA3-HA vectors as indicated using standard molecular cloning. To generate USP35- and NRF2-expressing stable cell lines, *USP35* and *NFE2L2* cDNA was shuttled into the pCDH vector. For USP35 knockdown cell lines, shRNAs (target sequences: sh1, CCGACTGCTGTACGGTATAAA; sh2, CAGACACCCATGTTCATAAAT) were designed using the web-based Genetic Perturbation Platform (https://portals.broadinstitute.org/gpp/public). Synthesized DNA oligos were ligated into the pLKO-Tet-on backbone. For virus production, the expression constructs and lentiviral packaging plasmids (pMD2.G and psPAX2) were co-transfected into HEK293T cells using Lipofectamine 3000 reagent (Invitrogen) according to manufacturer's instructions. Two days after transfection, media containing viral particles were collected and used to infect renal cancer cells to generate stable cell lines that were selected with puromycin treatment as described previously [19].

RNA-seq analysis

Cultured 769-P cells stably transfected with pLKO-Tet-on constructs for inducible expression of USP35 shRNA (sh2) were either untreated (control) or treated with doxycycline at 1 μg/ml for 4 days to induce USP35 knockdown. Efficient knockdown of USP35 was confirmed by

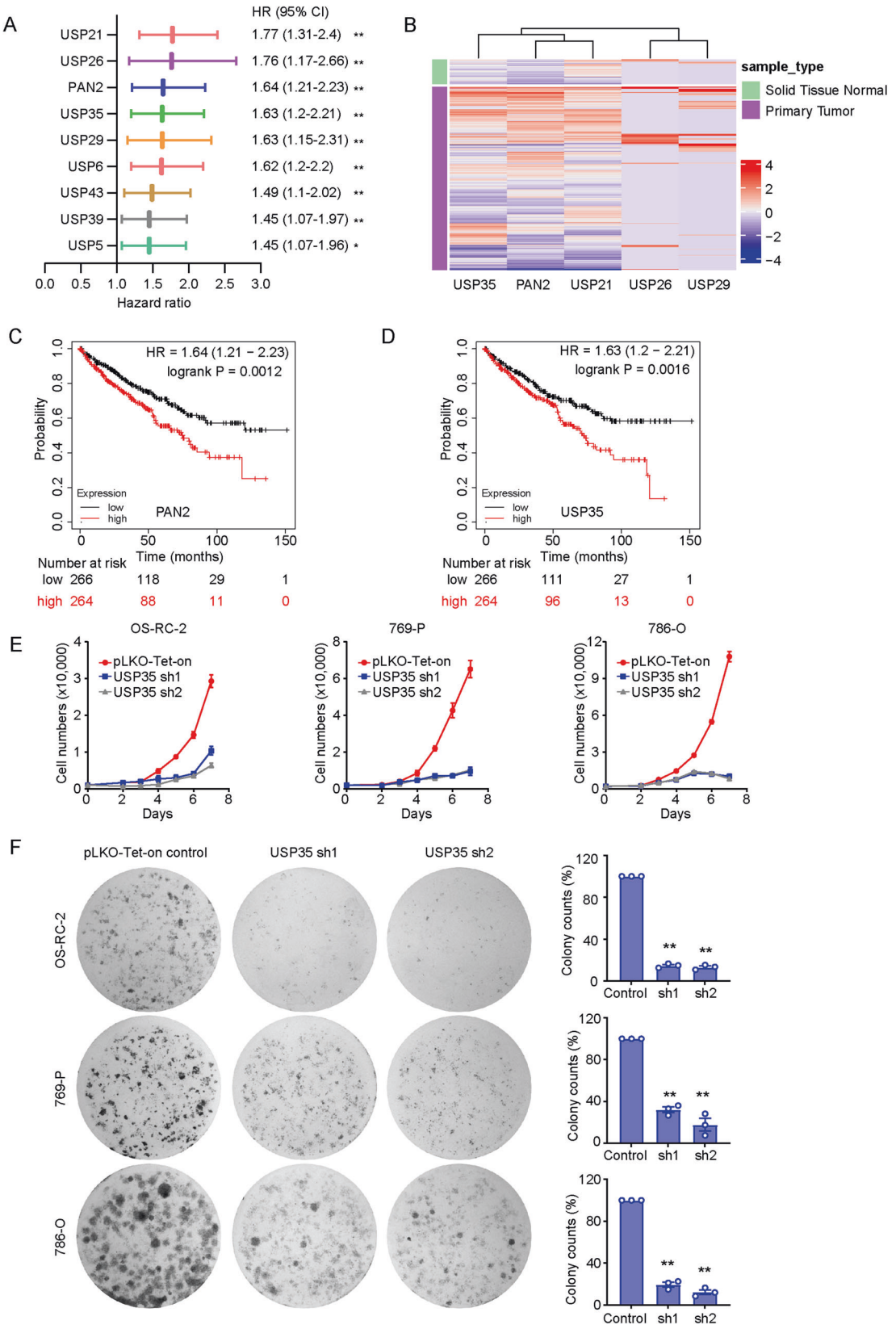

immunoblotting assays using parallel samples. Total RNA was harvested using the TRIzol reagent (Thermo Fisher) and then cleaned with a Qiagen RNAeasy Kit according to manufactures' instructions. Remaining DNA was removed by on-column digestion using RNase-free DNase. 2 µg of total RNA per condition ($n = 2$) were used for polyadenylated RNA extraction using the Illumina TruSeq Total RNA Sample Prep kit as per manufacturer's instruction. RNA integrity was evaluated with a Bioanalyzer (Agilent Technologies) before cDNA library construction with bar-coded ends. A

Fig. 1 USP35 expression predicts adverse prognosis of patients with RCC. A forest plot showing the HR values with 95% confidence intervals of top-listed USPs retrieved from the Kaplan–Meier Plotter database. **B** heatmap depicting the expression levels of indicated USPs in RCC and solid normal tissues. **C**, **D** survival curves based from the Kaplan–Meier Plotter database showing correlations between USP expression and patient outcomes. Patients were divided by the medians of USP expression. **E** growth curves of indicated RCC cells stably transfected with control vector (pLKO-Tet-on) or inducible USP35 shRNA constructs (sh1 and sh2). Cells were treated with doxycycline at 1 μg/ml that was applied 3 days before seeding and maintained during the whole experiment ($n = 3$). **F** stable cell lines described in **E** were used to perform colony formation assays. Representative images from three biological replicates were shown. Column charts on the right demonstrate quantification data ($n = 3$). All error bars represent the standard error of the mean (SEM), with ** denoting a p value of less than 0.01.

paired-end sequencing approach was adopted to obtain reads from both ends (150 bp) on an Illumina NovaSeq 6000 platform. Raw data (fastq) were initially processed to obtain clean reads through deleting reads with adapter, ploy-N, or low-quality sequences. Reference genome index was generated before clean data alignment to the reference genome using hisat2 (version 2.0.5). Gene expression analysis was conducted using featureCounts (version 1.5.0-p3), and fragments per kilo-base of exon per million fragments mapped (FPKM) values were calculated for each sample. Differentially expressed genes were assessed using the limma package from R (http://cran.r-project.org/), before enrichment analysis with the oncogenic signature gene sets from the Molecular Signatures Database (MSigDB).

Lipid peroxidation assay

A total of 2 × 10^5 cells were plated into each well of the 6-well plates and incubated overnight. The next day, cells were treated with the ferroptosis inducers for indicated times, before harvested by trypsinization. Then cells were incubated with 5 μM of BODIPY 581/591 C11 (D3861, Thermo Fisher) at 37 °C for 30 min. After PBS washes, fluorescence signals were collected using the Accuri C6 Plus flow cytometer (BD Biosciences) with a 488 nm laser.

Mouse xenograft model

Animal experimental procedures have been assessed and approved by the Institutional Animal Care and Use Committee at Dalian Medical University. Female Balb/c nude mice aged 6 weeks were obtained from Vital River Laboratory (Beijing, China). To generate xenografts of RCC, mice were randomized into two groups of 8 that were subcutaneously inoculated with 1 × 10^7 of OS-RC-2 cells stably transfected with USP35 Tet-on shRNA constructs or empty vector. After 7 days, mice were administered with doxycycline every day (20 mg/kg) to induce shRNA expression through oral gavage without blinding. Tumor size was measured using a caliper, and tumor volume was calculated as follows: (length×width^2) × (1/2).

Statistical analysis

The Graphpad Prism programme (version 8.0) was used to perform statistical analyses. Experiments were conducted with at least 3 biological replicates. Student's t-test (two-tailed) was used to compare the differences between groups. Results were demonstrated as mean ± standard error of the mean (SEM), with a p value less than 0.05 deemed as statistically significant difference.

RESULTS

USP35 expression correlates with poor prognosis in RCC

To examine the association of USPs with patient outcomes in RCC, we analyzed the RNA-seq and survival data from the TCGA repository integrated by the Kaplan-Meier Plotter (https://kmplot.com/analysis/) [20]. Hazard ratio (HR) with 95% confidence interval (CI) and log-rank P value for each USP were retrieved and summarized in Supplementary Table 1. We observed that 9 USPs (USP21, USP26, PAN2/USP52, USP35, USP29, USP6, USP43, USP39 and USP5 in descending order) were associated with an increased risk in RCC as identified by an HR value greater than 1 and P value smaller than 0.05 (Fig. 1A). Using TCGA sequencing data, we subsequently generated a heatmap to compare the expression of the top 5 USPs in RCC specimens and normal tissues. As demonstrated in Fig. 1B, relative to normal tissues, increased levels of PAN2 and USP35 in carcinoma specimens are seemingly more common as compared to the other 3 USPs. Therefore, we decided to investigate the implications of PAN2 and USP35.

As revealed by the survival curves that elevated expression of PAN2 or USP35 negatively correlates with patient prognosis (Fig. 1C, D), we speculated that knockdowns might affect the proliferation of RCC cells. Hence, we generated RCC cell lines stably expressing USP-specific shRNAs. Although the mRNA expression of PAN2 was efficiently depleted by both shRNAs, PAN2 silencing did not significantly influence RCC growth as revealed by growth curves and colony formation assays (Supplementary Fig. 1A–C). Regarding USP35, RCC cell lines with stable USP35 shRNA expression did not show significant knockdown. As such, we generated stable RCC cell lines using Tet-on-based inducible knockdown system (Supplementary Fig. 1D). Using these cells, we observed markedly obstructed cell propagation following doxycycline-induced USP35 depletion as revealed by growth curves and colony formation assays with OS-RC-2, 769-P and 786-O cells (Fig. 1E, F). Based on these observations, we decided to focus on USP35 for ensuing investigation.

USP35 stabilizes multiple IAP proteins to prevent apoptosis

USP35 was reported as an anti-apoptosis factor that antagonizes TRAIL- and staurosporine-induced apoptosis in HEK293 cells [21]. Consistently, we detected increased apoptosis in RCC cells following induced USP35 silencing, which was effectively blocked by the pan-caspase inhibitor Z-VAD-fmk (Supplementary Fig. 2A–C). To acquire mechanistic insights into its anti-apoptosis function, we follow the evidence of its *Drosophila* orthologue DeUBiquitinating-Apoptotic-Inhibitor (DUBAI, *CG8830*), which was shown to suppress apoptosis through stabilizing the *Drosophila* inhibitor of apoptosis protein (IAP) called DIAP1 [22]. Human IAP family consists of 8 members (BIRC1/NAIP, BIRC2/cIAP1, BIRC3/cIAP2, BIRC4/XIAP, BIRC5/Survivin, BIRC6/BRUCE/Apollon, BIRC7/Livin, and BIRC8/testis-specific IAP (Ts-IAP)) that are characterized by the existence of baculovirus IAP repeat (BIR) domains, and are widely recognized for their anti-apoptotic activities through inhibiting caspases [23].

To interrogate the potential regulation of IAPs by USP35, we co-expressed USP35 with each of 6 IAPs, including cIAP1, cIAP2, XIAP, Survivin, Livin, and BIRC8, using different tagging approach to optimize expression. As demonstrated in Fig. 2A, B, wild-type USP35 but not its catalytically inactive mutant C450A increased the levels of 5 IAPs (cIAP1, cIAP2, XIAP, Survivin, and Livin), indicative of potential DUB activity-dependent stabilizing effects (Supplementary Fig. 7). Subsequently, we selected 3 representative IAPs (cIAP2, XIAP, and Survivin) to perform coimmunoprecipitation assays with USP35 to investigate their association. As shown in Fig. 2C–E, exogenously expressed cIAP2, XIAP, and Survivin were readily detected in immunoprecipitated Flag-USP35 samples, suggesting interactions of USP35 with different IAPs (Supplementary Fig. 7). Accordingly, we speculated that the USP35-IAP association might be mediated through the BIR domains. We thus generated a series of BIR truncation mutants of cIAP2, XIAP, and Survivin before re-examined their associations with USP35. Interestingly, removal of two BIR domains in cIAP2 and XIAP dramatically reduced their association with USP35, while

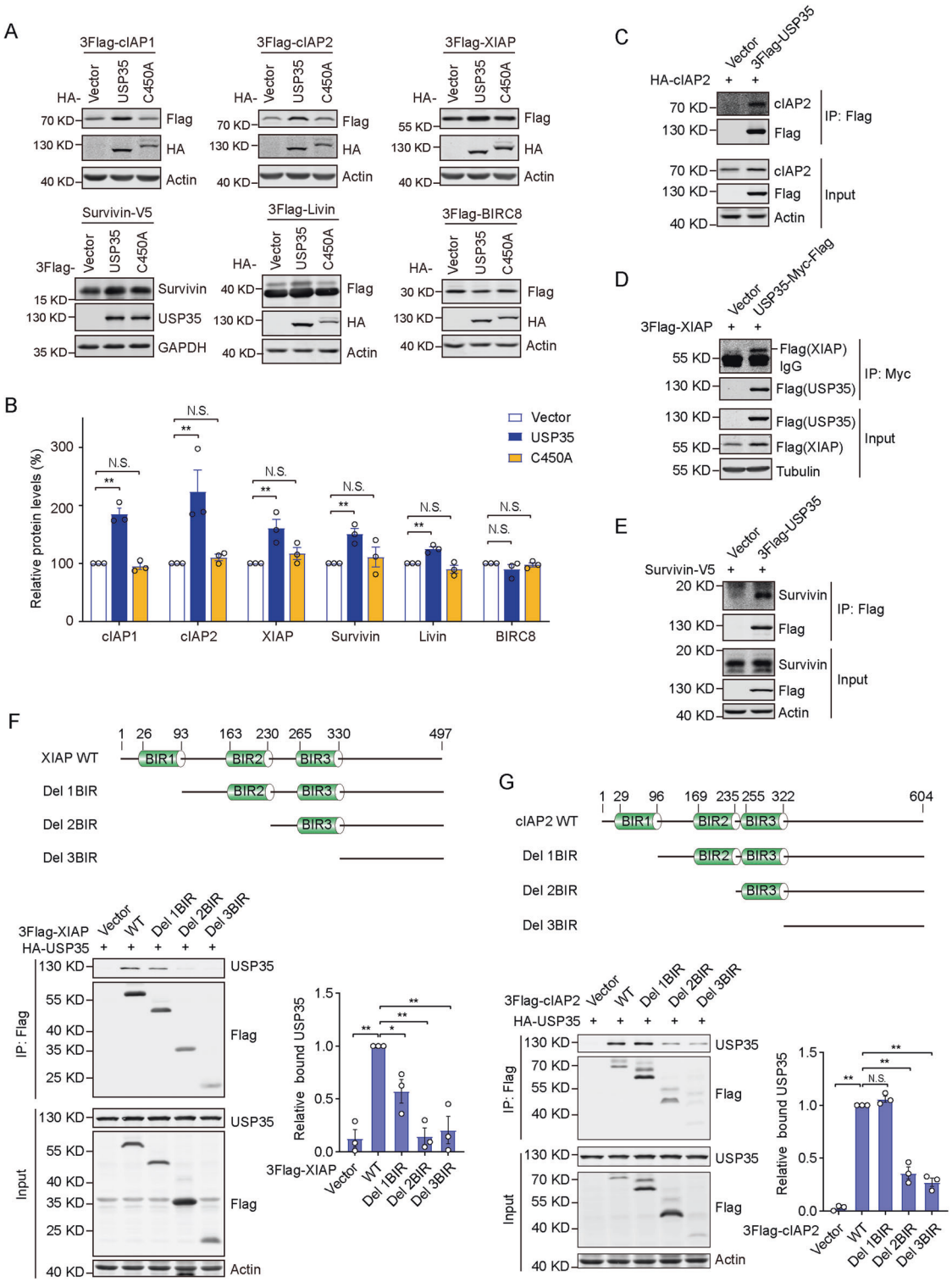

Fig. 2 USP35 stabilizes and associates with multiple IAP proteins. A HEK293T cells were co-transfected with USP35 wild-type, catalytically inactive C450A mutant, or vector control constructs along with plasmids expressing 6 separate IAP proteins (cIAP1, cIAP2, XIAP, Survivin, Livin, and BIRC8) with indicated tags for 48 h. Cell lysates were prepared and subjected to Western blotting analysis with indicated antibodies. Actin or GAPDH was probed to serve as loading controls. **B** quantification data of A from three biological repeats showing relative expression levels of IAP proteins as indicated. **C**–**E** HEK293T cells were co-transfected with IAP-expressing constructs as indicated together with control vector or USP35 plasmids for 48 h. Cell lysates were harvested, from which tagged USP35 proteins were immunoprecipitated using indicated antibodies. Immunoprecipitation (IP) samples were then analyzed by Western blotting in parallel with lysates (input) using indicated antibodies. **F**, **G** BIR domain-truncated mutants were generated for XIAP and cIAP2 as shown in the schematic illustration, which were used in co-immunoprecipitation assays with HA-tagged USP35. Samples were analyzed as in **C**. Column charts on the right show quantification data from three biological repeats. All error bars represent the standard error of the mean (SEM), with * and ** indicating a *p* value less than 0.05 and 0.01, respectively. N.S. means not significant.

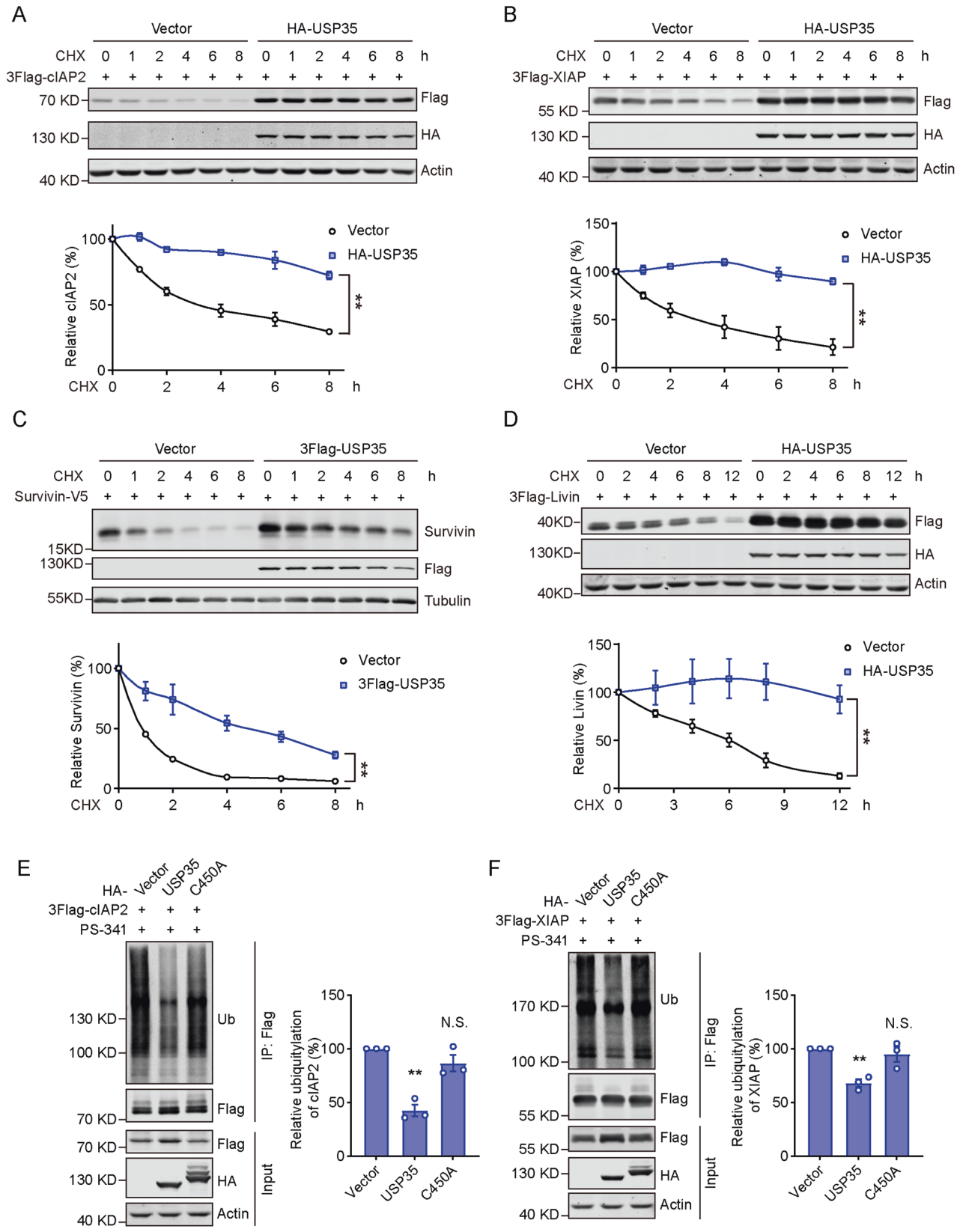

deletion of the only BIR domain in Survivin abolished their interaction (Fig. 2F, G; Supplementary Figs. 3A and 7). Therefore, our findings suggest that the BIR domains in IAPs play a dominant role in their association with USP35.

We next investigated the influence of USP35 on the stability of exogenously-expressed IAPs. Results from cycloheximide chase experiments revealed that USP35 markedly decelerated the turnover of cIAP1, cIAP2, XIAP, Survivin, and Livin, without

Fig. 3 USP35 maintains the stability and abates the ubiquitylation of IAP proteins. A–D HEK293T cells were co-transfected with USP35 or vector control constructs along with plasmids expressing indicated IAP proteins (cIAP2, XIAP, Survivin, and Livin) for 48 h, before incubation with 50 μg/ml of cycloheximide (CHX) for indicated times. Prepared lysates were analyzed by Western blotting assays using indicated antibodies. Actin and Tubulin blots show equal loading of samples. Degradation curves below show the turnover of corresponding IAP proteins summarized from three biological replicates. **E**, **F** HEK293T cells were transfected with indicated constructs as abovementioned, and treated with the proteasome inhibitor PS-341 at 500 nM for 6 h. Flag-tagged cIAP2 (**E**) and XIAP (**F**) proteins were immunoprecipitated with anti-Flag antibodies. IP samples were processed for immunoblotting assays along with lysates using indicated antibodies. Actin blots show equal loading. Column charts on the right show quantification data of relative ubiquitylation signals from three biological repeats. All error bars represent the standard error of the mean (SEM), and ** indicates a p value less than 0.01 while N.S. means not significant.

significantly affecting that of BIRC8 (Fig. 3A–D; Supplementary Fig. 3B, C; Supplementary Fig. 7). Subsequently, we examined ubiquitylation on immunoprecipitated IAPs in cells expressing wild-type or the catalytically-inactive C450A. As shown in Fig. 3E, F, wild-type USP35 effectively reduced the ubiquitin signal on immunoprecipitated cIAP2 and XIAP, while the C450A mutant refrained from affecting their ubiquitylation status (Supplementary Fig. 7).

Having confirmed its IAP-stabilizing effects, we then investigated the influence of USP35 knockdown on the endogenous abundance and turnover of IAPs. Using stable RCC cells with inducible USP35 knockdown, we examined endogenous levels of cIAP1, cIAP2, XIAP, Survivin, and Livin. Although the knockdown efficiency of USP35 was about 50% in OS-RC-2 and 769-P cells, the endogenous levels of cIAP2, Survivin, and Livin in both cell lines as well as those of XIAP in 769-P cells were evidently decreased following USP35 silencing, while cIAP1 expression remained relatively stable (Fig. 4A, B; Supplementary Fig. 7). Consistently, the endogenous levels of cIAP1, XIAP, Survivin, and Livin were effectively elevated with USP35 overexpression (Supplementary Figs. 4A–C and 7). Furthermore, in subsequent cycloheximide chase experiments, we observed that USP35 knockdown resulted in significantly increased turnover of endogenous cIAP2, XIAP, Survivin, and Livin (Fig. 4C; Supplementary Figs. 4D and 7). These observations suggest that, although USP35 exerts deubiquitylase function to stabilize multiple IAPs, the endogenous levels of various IAPs display differential sensitivity towards USP35 depletion. As expected, IAP knockdowns significantly enhanced cellular apoptosis in OS-RC-2 cells (Supplementary Fig. 5A, B). Taken together, our findings suggest that USP35 safeguards RCC against apoptosis through stabilizing multiple IAPs.

USP35 catalyzes NRF2 deubiquitylation

To explore additional functions of USP35, we conducted transcriptomic profiling of 769-P cells following induced USP35 depletion. Interestingly, oncogenic signature enrichment analysis of differentially expressed genes revealed that the *NFE2L2* gene set was among the top-listed (Fig. 5A). *NFE2L2* encodes for NRF2 that is an oxidative stress-responsive regulator vital for redox homeostasis [24]. Although NRF2 RNA levels were not reduced by USP35 silencing in RNA-seq analysis (Supplementary Table 2), we detected dramatic decreases of endogenous NRF2 protein abundance in OS-RC-2, 769-P and 786-O cells using immunoblotting assays following induced USP35 knockdown (Fig. 5B; Supplementary Fig. 7). Consistently, USP35 overexpression demonstrates a dose-dependent stabilizing effect on exogenously expressed NRF2 (Fig. 5C; Supplementary Fig. 7). In subsequent cycloheximide chase experiments, USP35 overexpression dramatically decelerated the turnover of HA-tagged NRF2 in HEK293T cells (Fig. 5D; Supplementary Fig. 7). Moreover, NRF2 was readily detected in USP35 immunoprecipitations, suggesting association between these proteins (Fig. 5E; Supplementary Fig. 7). Taken together, these findings strongly indicate the NRF2-stabilizing effect of USP35 in RCC cells.

NRF2 protein levels are kept in check closely by the ubiquitin proteasome system [25, 26]. Kelch-like ECH-associated protein-1 (Keap1) is recognized as the predominant factor governing NRF2 ubiquitylation by integrating into the cullin-3-Rbx1 ubiquitin ligase complex [27–31]. Accordingly, we investigated the influence of USP35 on NRF2 ubiquitylation and conducted a series of immunoprecipitation assays. As demonstrated in Fig. 5F, Keap1 overexpression markedly enhanced ubiquitylation signals on immunoprecipitated NRF2, while the expression of wild-type but not the C450A mutant of USP35 dramatically diminished NRF2 ubiquitylation under conditions with or without Keap1 overexpression (Supplementary Fig. 7). Collectively, these findings conclude that USP35 maintains NRF2 protein abundance by acting as a deubiquitylating enzyme to counteract ubiquitylation-mediated NRF2 degradation.

USP35 protects RCC cells from ferroptosis

Ferroptosis is a recently identified novel form of regulated cell death, which is characterized by iron-dependent lipid peroxidation driven predominantly by oxidative stresses [32, 33]. Accumulating evidence has linked ferroptosis to multiple diseases including cancer and suggests it as a promising vulnerability to target human malignancies [34, 35]. Notably, the master redox regulator NRF2 has been intimately implicated in ferroptosis and revealed as a vital defense mechanism to antagonize ferroptotic cell death [36]. Based on our findings that NRF2 protein levels are governed by the DUB activity of USP35, we speculated that USP35 might also be incorporated into the cellular defense system against ferroptosis. To test this hypothesis, we examined the contribution of USP35 to cellular ferroptosis in RCC cells that are amenable to the GPX4 inhibitor RSL3-induced ferroptosis and exhibit sensitivity towards alterations in NRF2 levels (Supplementary Fig. 6A–D; Supplementary Fig. 7) [37].

Using inducible USP35 knockdown cell lines, we observed cell morphology and propidium iodide (PI) staining following RSL3 treatment. As shown in Fig. 6A, B, USP35 silencing markedly enhanced RSL3-triggered cellular ferroptosis in OS-RC-2 and 769-P cells before the apparent occurrence of apoptosis, which was effectively blocked by the ferroptosis inhibitor ferrostatin-1. As expected, decreased NRF2 abundance imposed by induced USP35 knockdown resulted in elevated cellular ROS levels in both OS-RC-2 and 769-P cells as revealed by dichlorofluorescin (DCF) assays (Fig. 6C). In addition, under steady-state conditions without ferroptosis induction, induced USP35 knockdown also led to increased lipid ROS levels detected by C11-BODIPY assays in both RCC cells (Fig. 6D, E). Importantly, in accordance with markedly increased sensitivity to ferroptosis, induced USP35 silencing dramatically aggravated the RSL3-incurred lipid peroxidation in 769-P cells (Fig. 7A). Therefore, our findings corroborate the protective effect of USP35 against ferroptosis in RCC.

NRF2 mediates the anti-ferroptosis function of USP35

A recent study by Cheng and colleagues also linked USP35 to ferroptosis in lung cancer through regulating ferroportin stability [38]. Accordingly, we examined the protein levels of ferroportin in RCC cells depleted of USP35. As demonstrated in Supplementary Figs. 6G and 7, USP35 silencing refrained from affecting the protein abundance of ferroportin in RCC cells, thus suggesting a

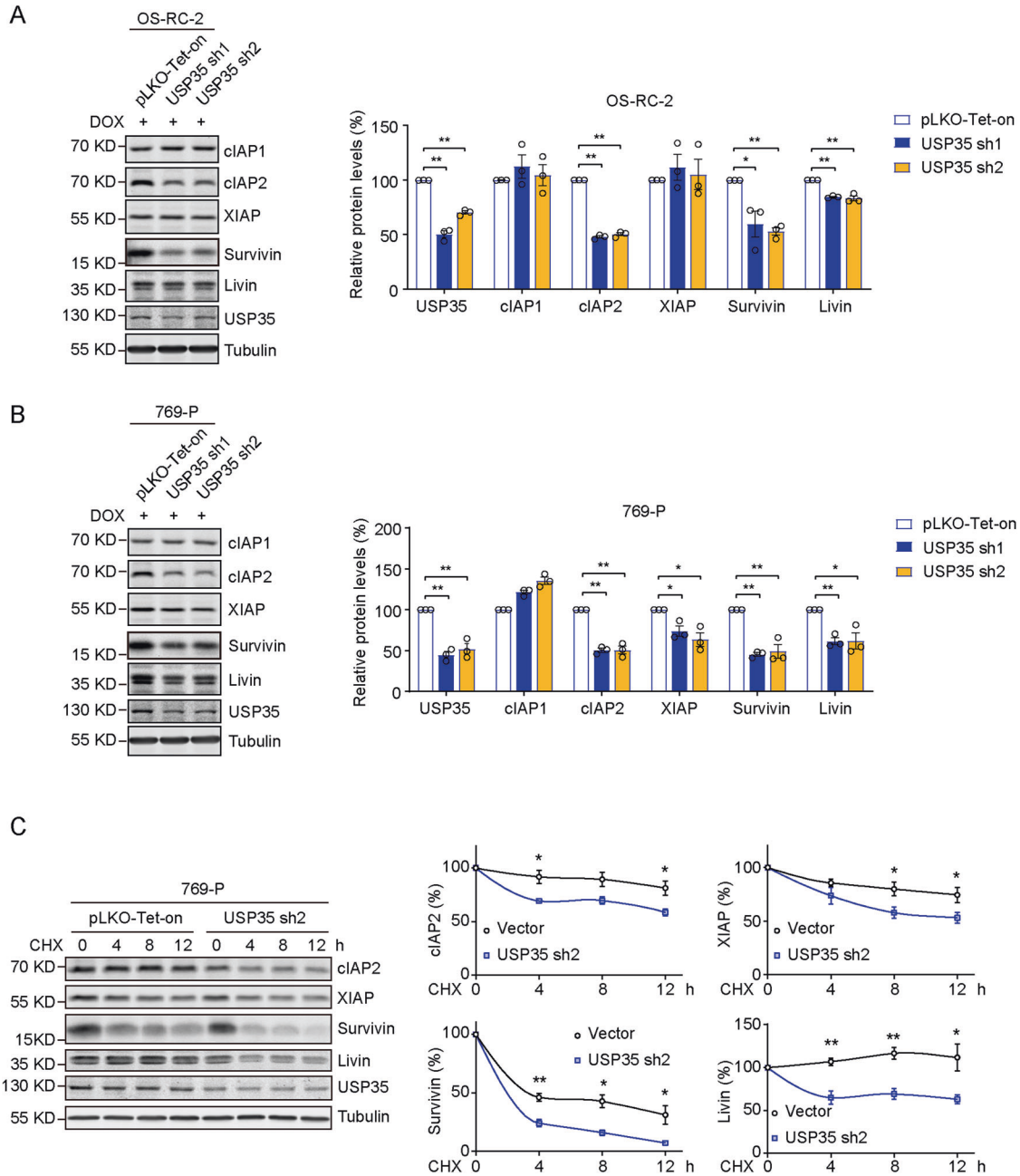

Fig. 4 USP35 regulates the expression levels and turnover of endogenous IAP proteins. A, **B** OS-RC-2 and 796-P cells stably transfected with control vector (pLKO-Tet-on) or inducible USP35 shRNA constructs (two separate sequences: sh1 and sh2) were treated with doxycycline at 1 μg/ml for 5 days to knock down USP35 expression. Cell lysates were prepared and processed for Western blotting analysis using indicated antibodies. Tubulin was also probed to confirm equal loading. Column charts on the right show quantification data of relative levels for USP35 and various IAP proteins from 3 biologically independent repeats. **C** cultured 769-P stable cell lines were treated as in **B** to induce USP35 silencing and subsequently incubated with 50 μg/ml of cycloheximide (CHX) for indicated times. Cell lysates were analyzed with Western blotting using indicated antibodies. Tubulin was probed to confirm equal loading. Turnover curves on the right show quantification data from 3 independent repeats for each IAP protein. All error bars represent the standard error of the mean (SEM). * and **, *p* value smaller than 0.05 and 0.01, respectively.

distinctive approach adopted by USP35 to antagonize ferroptosis in RCC. To confirm that the anti-ferroptosis function of USP35 is exerted through regulating NRF2, we rescued NRF2 protein expression in USP35 knockdown cells. As shown in Fig. 7B, NRF2 overexpression in OS-RC-2 cells with USP35 silencing markedly elevated the expression of its downstream target aldo-keto reductase family 1 member B10 (AKR1B10), suggesting effective transcriptional activity conferred by NRF2 expression (Supplementary Fig. 7). Importantly, USP35-depleted cells with NRF2 overexpression were indeed recorded with significantly attenuated ferroptotic cell death following RSL3 treatment (Fig. 7C, D). Hence, these findings collectively infer that USP35 restricts ferroptosis in RCC via stabilizing NRF2.

USP35 silencing diminishes tumorigenesis in nude mice

Given that USP35 is closely implicated in RCC survival through precluding regulated cell deaths, we investigated the effects of USP35 silencing on RCC xenograft formation in immunodeficient

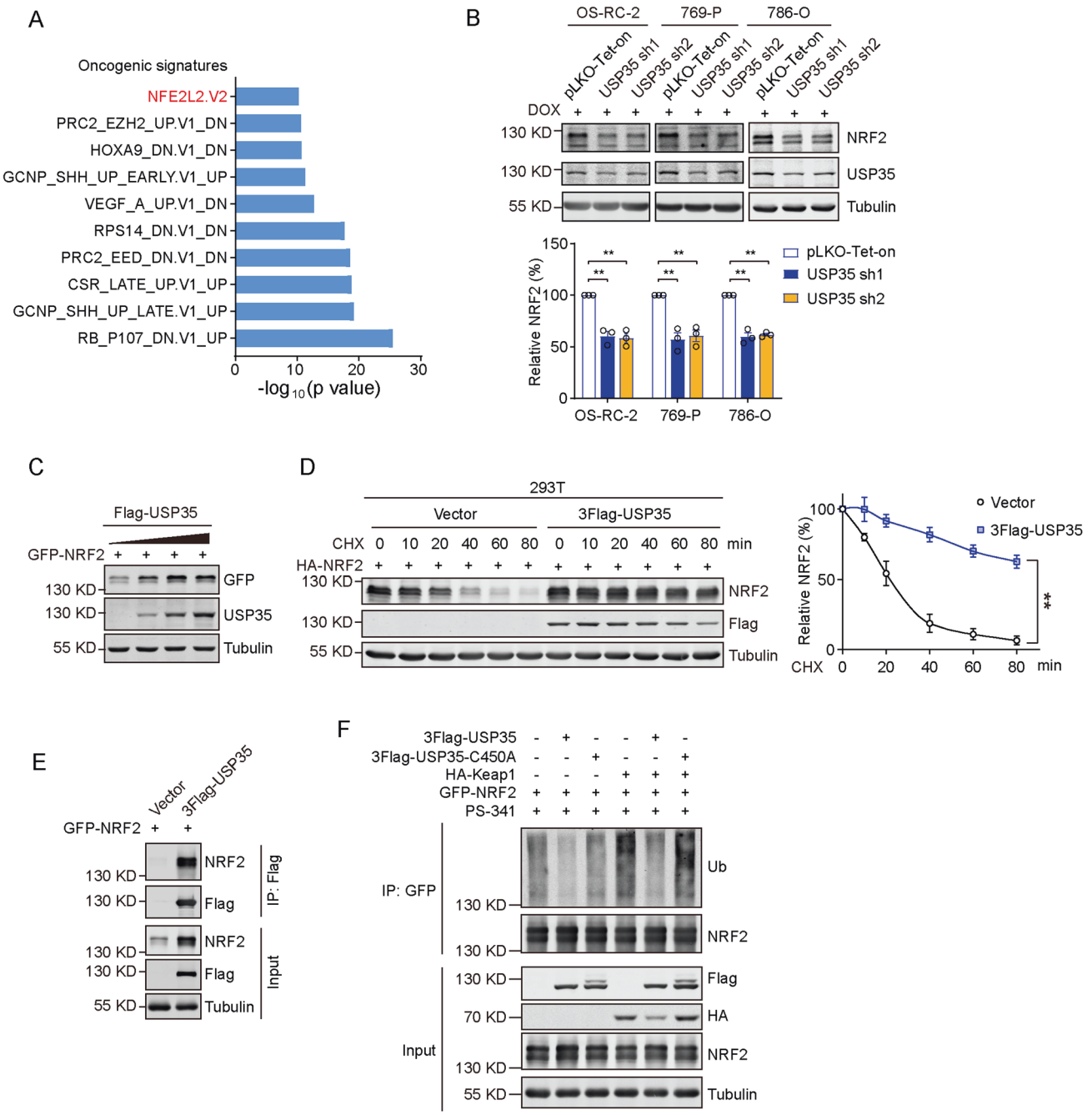

Fig. 5 USP35 silencing leads to NRF2 downregulation in RCC cells. A Bar chart demonstrating oncogenic signature gene set enrichment analysis of transcriptomic data ($n = 2$). **B** cultured OS-RC-2, 769-P, and 786-O cells with stable transfection of control vector (pLKO-Tet-on) or inducible USP35 shRNA constructs (sh1 and sh2) were treated with doxycycline (1 μg/ml, 4 days) to induce USP35 depletion. Cell lysates were harvested and analyzed by Western blotting with anti-NRF2 and anti-USP35 antibodies. Tubulin was probed to ensure equal loading. Column chart below shows quantification of relative NRF2 abundance from 3 biological replicates. **C** HEK293T cells were co-transfected with plasmids expressing GFP-tagged NRF2 (250 ng) and Flag-tagged USP35 (0, 50, 200, 750 ng) for 36 h. The amounts of total plasmid per condition were made equal with empty vector. Harvested lysates were subjected to Western blot assays with anti-GFP and anti-USP35 antibodies. Tubulin blot shows equal loading. **D** HEK293T cells were co-transfected with HA-NRF2 and 3Flag-USP35 constructs. Cells were treated with cycloheximide (CHX, 50 μg/ml) for indicated times and lysed, followed by immunoblotting analysis with anti-NRF2 and anti-Flag antibodies. Tubulin was probed to ensure equal loading. Degradation curve on the right shows the quantification of NRF2 turnover from 3 biological repeats. **E** HEK293T cells were co-transfected with indicated constructs and cell lysates was acquired to carry out immunoprecipitation assays using anti-Flag antibody to pull down USP35. IP and lysate (input) samples were analyzed by Western blotting using indicated antibodies. **F** cultured HEK293T cells were co-transfected with GFP-NRF2 construct in combination with plasmids expressing 3Flag-USP35 wild-type or catalytically inactive C450A mutant, or HA-Keap1 as indicated. Following PS-341 treatment (500 nM, 7 h), cell lysates were harvested to conduct immunoprecipitation assays using anti-GFP antibody to enrich GFP-NRF2. Subsequently, IP and input samples were subjected to Western blotting analysis using indicated antibodies. All error bars represent standard error of the mean (SEM), with ** denoting p values less than 0.01.

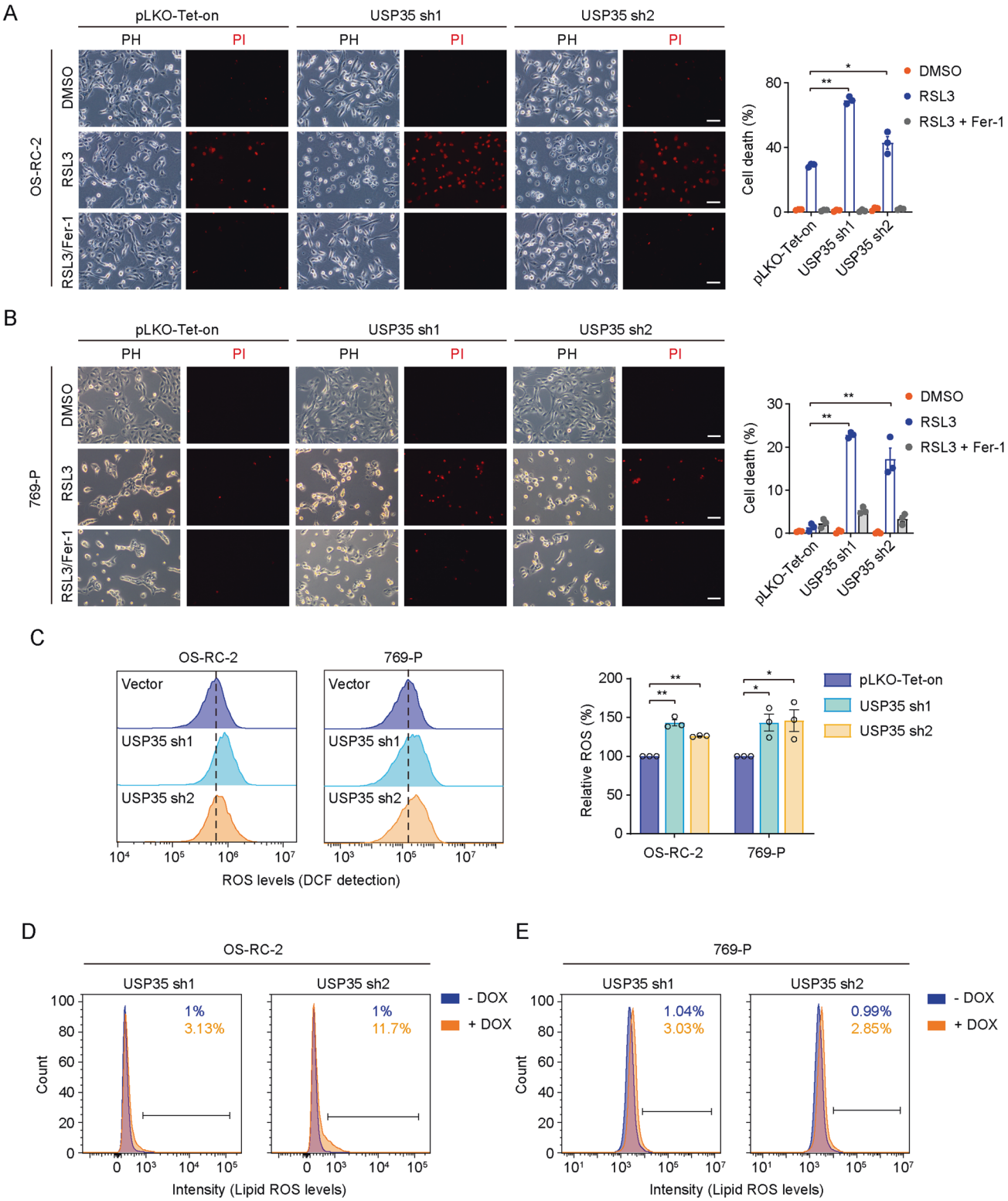

mice. To this end, we subcutaneously inoculated OS-RC-2 cells with inducible USP35 knockdown into female nude mice. USP35 silencing was induced by doxycycline. As demonstrated in Fig. 8A–C, although the growth of xenografts formed by OS-RC-2 vector control cells was uneven, induced USP35 silencing dramatically hindered the formation of xenografts by OS-RC-2 Tet-on-shUSP35 cells. Therefore, our in vivo findings with xenograft mouse models further corroborate the tumor-supporting role of USP35 in the tumorigenesis of RCC. Taken together, our observations conclude that USP35 demonstrates a tumor-protecting role by antagonizing the occurrence of apoptotic and ferroptotic cell deaths, through catalytically maintaining the levels of multiple IAP proteins and the redox regulator NRF2, respectively (Fig. 8D).

Fig. 6 USP35 silencing renders RCC cells increased sensitivity to ferroptosis. A, **B** OS-RC-2 and 769-P cell lines stably transfected with control vector (pLKO-Tet-on) or inducible USP35 shRNA constructs (sh1 and sh2) were treated with doxycycline (1 μg/ml, 4 days) to silence USP35 expression. After PBS washes to remove the small amounts of apoptotic cells, OS-RC-2 cells were treated with RSL3 (2 μM) in the presence or absence of ferrostatin-1 (Fer-1, 2 μM) for 3 h, while 769-P cells were treated with RSL3 (20 μM) in the presence or absence of ferrostatin-1 (10 μM) for 14 h. Following treatment, dead cells were stained with propidium iodide (PI) and immediately examined under a fluorescence microscope. Representative images from 3 biological replicates were shown. PH, phase contrast views. Scale bar = 50 μm. Column charts on the right show the quantification of cell death from 3 independent biological repeats. **C** stable OS-RC-2 and 769-P cell lines were treated with doxycycline to induce USP35 knockdown as abovementioned. Harvested cells were treated with dichlorofluorescin diacetate (DCFH-DA) and processed for flow cytometry assays to detect cellular ROS levels as described in the method section. Column chart on the right shows the quantification data of relative ROS levels from 3 biological replicates. **D**, **E** OS-RC-2 and 769-P cells with stable transfection of inducible USP35 shRNA constructs with or without doxycycline treatment (1 μg/ml, 4 days) were harvested for C11-BODIPY staining-based lipid peroxidation assays using flow cytometry. Representative histograms with quantification demonstrate relative lipid ROS levels in cells with or without induced USP35 knockdown. All error bars represent standard error of the mean (SEM), with * and ** denoting *p* values less than 0.05 and 0.01, respectively.

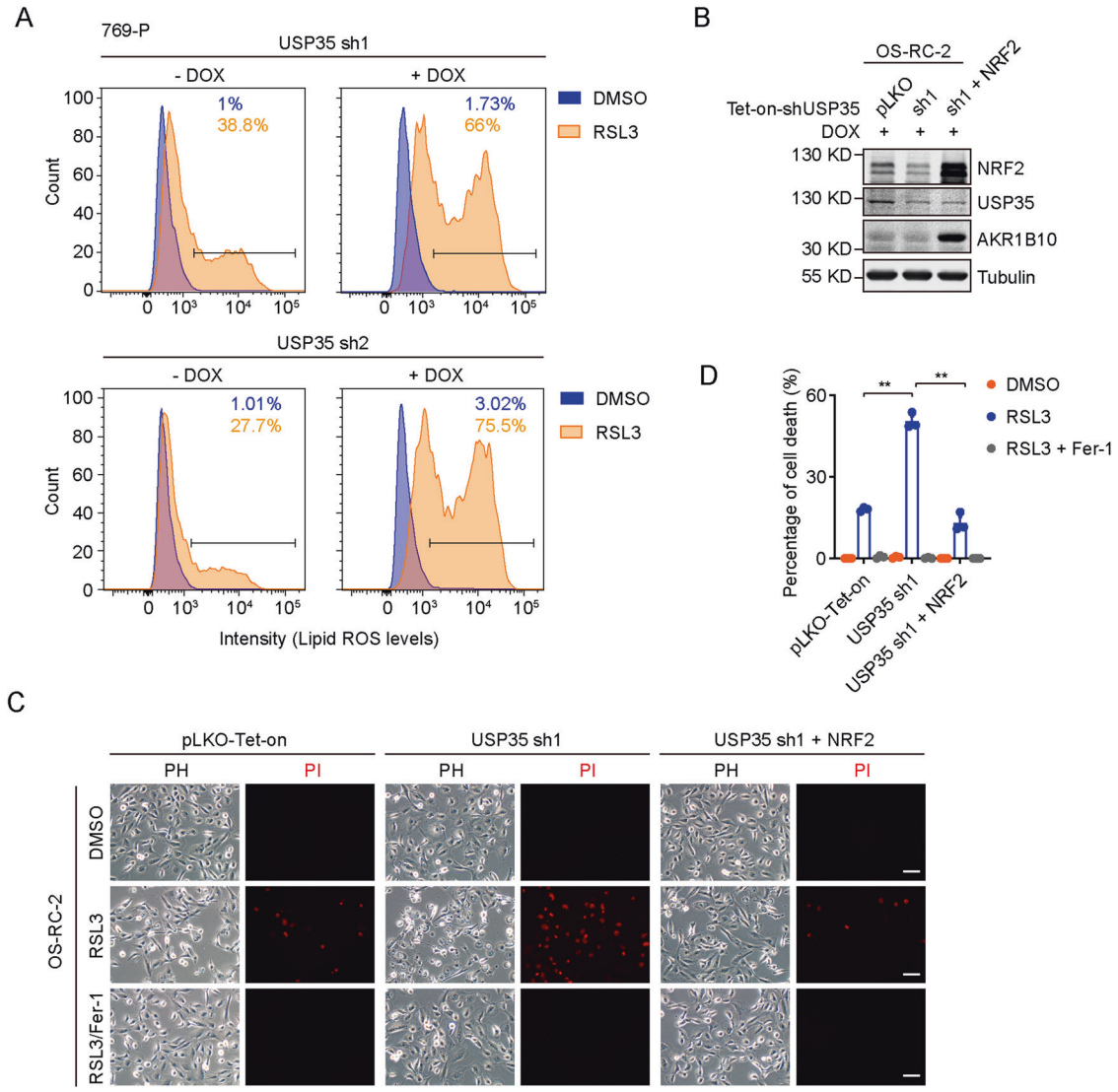

Fig. 7 The overexpression of NRF2 alleviates increased ferroptotic cell death imposed by USP35 silencing. A cultured 769-P cells stably transfected with inducible USP35 shRNA construct with or without doxycycline treatment (1 μg/ml, 5 days) were exposed to RSL3 (5 μM, 1 h) to induce ferroptosis or DMSO as vehicle control. Following treatment, cells were processed for lipid peroxidation analysis (C11-BODIPY staining) using flow cytometry. Representative histograms with quantification data show relative lipid ROS levels in cells with or without induced USP35 silencing in the presence or absence of RSL3. **B** OS-RC-2 cell lines stably transfected with control vector or inducible USP35 shRNA construct, or with additional stable expression of NRF2 as indicated were treated with doxycycline to induce USP35 depletion (1 μg/ml, 4 days). Cells were lysed to examine protein expression by performing Western blotting assays using indicated antibodies. **C** OS-RC-2 cells were treated as in B and then exposed to RSL3 (2 μM) or DMSO as control in the presence or absence of ferrostatin-1 (Fer-1, 2 μM) for 2.5 h. Immediately after treatment, cells were stained with PI and examined under a fluorescence microscope. Representative images from 3 biological repeats were demonstrated. PH, phase contrast views. Scale bar = 50 μm. **D** quantification data of **C** showing percentages of cell death calculated from each condition ($n = 3$). Error bars represent standard error of the mean (SEM), with ** indicating *p* values less than 0.01.

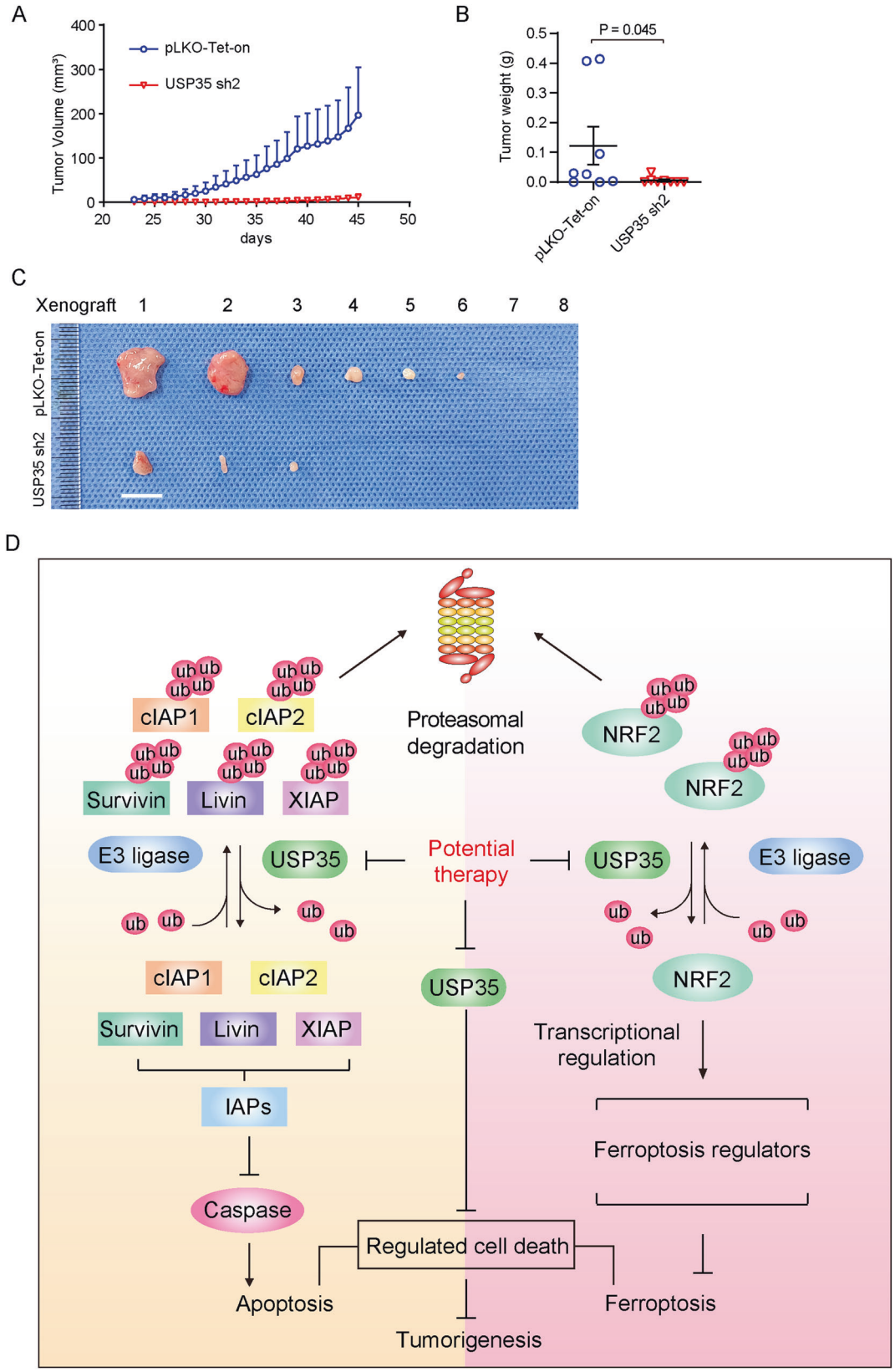

DISCUSSION

Resisting cell death is recognized as a pivotal hallmark of human malignancies [39]. In doing so, cancer cells have developed the capability to mount an effective defense against various cell death modalities by deploying cellular protection mechanisms. Accordingly, such dependence upon intrinsic pro-survival pathways confers lethal vulnerabilities and provides potential therapeutic approaches for pharmacological intervention in cancer treatment

Fig. 8 The tumor-promoting role of USP35 in RCC. A OS-RC-2 cells stably transfected with control vector or inducible USP35 shRNA construct were inoculated into athymic nude mice to allow xenograft formation. The volumes of tumor xenografts were measured and plotted. **B** tumor weight of resected xenograft tumors from two groups were examined and plotted. *P* value was calculated by performing Student's *t* test ($n = 8$). Error bars represent the standard error of the mean (SEM). **C** image showing resected xenograft tumors, with some blanks meaning no xenograft formation observed. **D** cartoon diagram depicting current working model, in which USP35 functions to deubiquitylate multiple IAP proteins and NRF2 to maintain their cellular abundance and therefore preclude the occurrence of apoptotic and ferroptotic cell death. As such, pharmacological targeting of USP35 in RCC holds potential to serve as a therapeutic strategy through the induction of regulated cell death.

[40, 41]. Induced cell death exemplified by apoptosis and necrosis has proved to play a fundamental role in the efficacy of cancer treatment regimens such as chemotherapy, radiotherapy, and targeted therapy. Importantly, extensive research has led to the successful approval of the BCL-2 inhibitor venetoclax by the US Food and Drug Administration (FDA) in cancer treatment, which functions by directly inducing apoptosis.

While our understanding of the molecular underpinnings of cellular apoptotic regulation has matured to allow the development of cancer therapies, new forms of regulated cell death also surfaced and thus offer novel opportunities to combat cancer. Ferroptosis is a recently identified cell death modality closely associated with cellular oxidative stresses, with emerging implications in tumorigenesis [35]. Accumulating evidence has experimentally confirmed that ferroptosis induction effectively suppressed the growth and progression of multiple types of cancer, thus providing a cornerstone allowing further investigation into its significance in tumorigenesis and potential therapy.

Through analyzing TCGA patient prognosis and subsequent phenotypic assays with RCC cells, we corroborated the tumor-promoting roles of USP35. Further biochemical characterizations revealed its stabilizing effects towards multiple IAP proteins. DUBs have previously been associated with the regulation of IAPs, including the control of XIAP turnover by USP11, the stabilization of c-IAP1 by OTUB1, and the deubiquitylating activity-independent regulation of c-IAP1 and c-IAP2 expression by USP19 [42–44]. Therefore, these findings suggest certain degree of redundancy in the post-translational control of IAP proteins, indicative of their essential roles in counteracting apoptosis. Nevertheless, it is intriguing that USP35 is capable of stabilizing multiple IAPs, which is likely linked to its competency to maintain cellular survival. In accordance with our findings, another study by Li and colleagues recently reported USP35-mediated stabilization of Survivin during the preparation of this manuscript [45].

In addition, our investigation uncovers another vital function of the multifaceted USP35 that is acquired by RCC cells to preclude ferroptosis. Through NRF2 stabilization, USP35 is intertwined with cellular anti-oxidation defense system that functions to keep cellular ROS and lipid peroxidation in check so as to avert oxidative stress-triggered cell damages including ferroptosis. The cellular anti-oxidation system has long been considered as a therapeutic target to battle against human malignancies [24]. Taken together, our findings disclose the tumor-protective roles of USP35 by precluding apoptosis and ferroptosis, which is mediated through maintaining the stability of multiple IAPs and NRF2, respectively. USP35 that is categorized as a cysteine protease provides a potential actionable target for pharmacological intervention to tackle with cellular defense mechanisms, which are vital in tumorigenesis and drug resistance [46]. As no small molecular inhibitors against USP35 have been reported until now, its development remains an intriguing frontier and warrants further investigation.

DATA AVAILABILITY

The data supporting the findings of this study are included in the article and supplementary files. RNA-seq data have been deposited in Gene Expression Omnibus of NCBI (accession code GSE216154).

REFERENCES

1. Sung H, Ferlay J, Siegel RL, Laversanne M, Soerjomataram I, Jemal A, et al. Global Cancer Statistics 2020: GLOBOCAN Estimates of Incidence and Mortality Worldwide for 36 Cancers in 185 Countries. CA: a cancer J clinicians. 2021;71:209–49.
2. Motzer RJ, Bander NH, Nanus DM. Renal-cell carcinoma. N. Engl J Med. 1996;335:865–75.
3. Hsieh JJ, Purdue MP, Signoretti S, Swanton C, Albiges L, Schmidinger M, et al. Renal cell carcinoma. Nat Rev Dis Prim. 2017;3:17009.
4. Cohen P, Tcherpakov M. Will the ubiquitin system furnish as many drug targets as protein kinases? Cell 2010;143:686–93.
5. Huang X, Dixit VM. Drugging the undruggables: exploring the ubiquitin system for drug development. Cell Res. 2016;26:484–98.
6. Tokheim C, Wang X, Timms RT, Zhang B, Mena EL, Wang B, et al. Systematic characterization of mutations altering protein degradation in human cancers. Mol cell. 2021;81:1292–308.e11
7. Kandoth C, McLellan MD, Vandin F, Ye K, Niu B, Lu C, et al. Mutational landscape and significance across 12 major cancer types. Nature 2013;502:333–9.
8. Clark DJ, Dhanasekaran SM, Petralia F, Pan J, Song X, Hu Y, et al. Integrated Proteogenomic Characterization of Clear Cell Renal Cell Carcinoma. Cell 2019;179:964–83.e31
9. Dizman N, Philip EJ, Pal SK. Genomic profiling in renal cell carcinoma. Nat Rev Nephrol. 2020;16:435–51.
10. Clague MJ, Barsukov I, Coulson JM, Liu H, Rigden DJ, Urbe S. Deubiquitylases from genes to organism. Physiological Rev. 2013;93:1289–315.
11. Duns G, Hofstra RM, Sietzema JG, Hollema H, van Duivenbode I, Kuik A, et al. Targeted exome sequencing in clear cell renal cell carcinoma tumors suggests aberrant chromatin regulation as a crucial step in ccRCC development. Hum Mutat. 2012;33:1059–62.
12. Pena-Llopis S, Vega-Rubin-de-Celis S, Liao A, Leng N, Pavia-Jimenez A, Wang S, et al. BAP1 loss defines a new class of renal cell carcinoma. Nat Genet. 2012;44:751–9.
13. Hong K, Hu L, Liu X, Simon JM, Ptacek TS, Zheng X, et al. USP37 promotes deubiquitination of HIF2alpha in kidney cancer. Proc Natl Acad Sci USA. 2020;117:13023–32.
14. Clague MJ, Urbe S, Komander D. Breaking the chains: deubiquitylating enzyme specificity begets function. Nat Rev Mol cell Biol. 2019;20:338–52.
15. Chen D, Ning Z, Chen H, Lu C, Liu X, Xia T, et al. An integrative pan-cancer analysis of biological and clinical impacts underlying ubiquitin-specific-processing proteases. Oncogene 2020;39:587–602.
16. Liu S, Wang T, Shi Y, Bai L, Wang S, Guo D, et al. USP42 drives nuclear speckle mRNA splicing via directing dynamic phase separation to promote tumorigenesis. Cell death Differ. 2021;28:2482–98.
17. Wu Y, Zhang Y, Wang D, Zhang Y, Zhang J, Zhang Y, et al. USP29 enhances chemotherapy-induced stemness in non-small cell lung cancer via stabilizing Snail1 in response to oxidative stress. Cell death Dis. 2020;11:796.
18. Sun Q, Zhang J, Li X, Yang G, Cheng S, Guo D, et al. The ubiquitin-specific protease 8 antagonizes melatonin-induced endocytic degradation of MT(1) receptor to promote lung adenocarcinoma growth. J Adv Res. 2022;41:1–12.
19. Zhang J, Liu S, Li Q, Shi Y, Wu Y, Liu F, et al. The deubiquitylase USP2 maintains ErbB2 abundance via counteracting endocytic degradation and represents a therapeutic target in ErbB2-positive breast cancer. Cell death Differ. 2020;27:2710–25.
20. Nagy A, Munkacsy G, Gyorffy B. Pancancer survival analysis of cancer hallmark genes. Sci Rep. 2021;11:6047.
21. Leznicki P, Natarajan J, Bader G, Spevak W, Schlattl A, Abdul Rehman SA, et al. Expansion of DUB functionality generated by alternative isoforms - USP35, a case study. J Cell Sci. 2018;131:jcs212753.
22. Yang CS, Sinenko SA, Thomenius MJ, Robeson AC, Freel CD, Horn SR, et al. The deubiquitinating enzyme DUBAI stabilizes DIAP1 to suppress Drosophila apoptosis. Cell death Differ. 2014;21:604–11.
23. Kumar S, Fairmichael C, Longley DB, Turkington RC. The Multiple Roles of the IAP Super-family in cancer. Pharmacol therapeutics. 2020;214:107610.

24. Hayes JD, Dinkova-Kostova AT, Tew KD. Oxidative Stress in Cancer. Cancer cell. 2020;38:167–97.
25. Hayes JD, Chowdhry S, Dinkova-Kostova AT, Sutherland C. Dual regulation of transcription factor Nrf2 by Keap1 and by the combined actions of beta-TrCP and GSK-3. Biochemical Soc Trans. 2015;43:611–20.
26. Baird L, Yamamoto M. The Molecular Mechanisms Regulating the KEAP1-NRF2 Pathway. Mol Cell Biol. 2020;40:e00099-20.
27. McMahon M, Itoh K, Yamamoto M, Hayes JD. Keap1-dependent proteasomal degradation of transcription factor Nrf2 contributes to the negative regulation of antioxidant response element-driven gene expression. The. J Biol Chem. 2003;278:21592–600.
28. Itoh K, Wakabayashi N, Katoh Y, Ishii T, O'Connor T, Yamamoto M. Keap1 regulates both cytoplasmic-nuclear shuttling and degradation of Nrf2 in response to electrophiles. Genes Cells: devoted Mol Cell mechanisms. 2003;8:379–91.
29. Kobayashi A, Kang MI, Okawa H, Ohtsuji M, Zenke Y, Chiba T, et al. Oxidative stress sensor Keap1 functions as an adaptor for Cul3-based E3 ligase to regulate proteasomal degradation of Nrf2. Mol Cell Biol. 2004;24:7130–9.
30. Cullinan SB, Gordan JD, Jin J, Harper JW, Diehl JA. The Keap1-BTB protein is an adaptor that bridges Nrf2 to a Cul3-based E3 ligase: oxidative stress sensing by a Cul3-Keap1 ligase. Mol Cell Biol. 2004;24:8477–86.
31. Zhang DD, Lo SC, Cross JV, Templeton DJ, Hannink M. Keap1 is a redox-regulated substrate adaptor protein for a Cul3-dependent ubiquitin ligase complex. Mol Cell Biol. 2004;24:10941–53.
32. Dixon SJ, Lemberg KM, Lamprecht MR, Skouta R, Zaitsev EM, Gleason CE, et al. Ferroptosis: an iron-dependent form of nonapoptotic cell death. Cell 2012;149:1060–72.
33. Stockwell BR, Jiang X. The Chemistry and Biology of Ferroptosis. Cell Chem Biol. 2020;27:365–75.
34. Tang D, Chen X, Kang R, Kroemer G. Ferroptosis: molecular mechanisms and health implications. Cell Res. 2021;31:107–25.
35. Chen X, Kang R, Kroemer G, Tang D. Broadening horizons: the role of ferroptosis in cancer. Nat Rev Clin Oncol. 2021;18:280–96.
36. Anandhan A, Dodson M, Schmidlin CJ, Liu P, Zhang DD. Breakdown of an Ironclad Defense System: The Critical Role of NRF2 in Mediating Ferroptosis. Cell Chem Biol. 2020;27:436–47.
37. Yang WS, SriRamaratnam R, Welsch ME, Shimada K, Skouta R, Viswanathan VS, et al. Regulation of ferroptotic cancer cell death by GPX4. Cell 2014;156:317–31.
38. Tang Z, Jiang W, Mao M, Zhao J, Chen J, Cheng N. Deubiquitinase USP35 modulates ferroptosis in lung cancer via targeting ferroportin. Clin Transl Med. 2021;11:e390.
39. Hanahan D, Weinberg RA. Hallmarks of cancer: the next generation. Cell 2011;144:646–74.
40. Galluzzi L, Vitale I, Aaronson SA, Abrams JM, Adam D, Agostinis P, et al. Molecular mechanisms of cell death: recommendations of the Nomenclature Committee on Cell Death 2018. Cell death Differ. 2018;25:486–541.
41. Diepstraten ST, Anderson MA, Czabotar PE, Lessene G, Strasser A, Kelly GL. The manipulation of apoptosis for cancer therapy using BH3-mimetic drugs. Nature Rev Cancer. 2021.
42. Zhou Z, Luo A, Shrivastava I, He M, Huang Y, Bahar I, et al. Regulation of XIAP Turnover Reveals a Role for USP11 in Promotion of Tumorigenesis. EBioMedicine 2017;15:48–61.
43. Koschel J, Nishanth G, Just S, Harit K, Kroger A, Deckert M, et al. OTUB1 prevents lethal hepatocyte necroptosis through stabilization of c-IAP1 during murine liver inflammation. Cell Death Differ. 2021;28:2257–75.
44. Mei Y, Hahn AA, Hu S, Yang X. The USP19 deubiquitinase regulates the stability of c-IAP1 and c-IAP2. The. J Biol Chem. 2011;286:35380–7.
45. Wang W, Lin H, Zheng E, Hou Z, Liu Y, Huang W, et al. Regulation of survivin protein stability by USP35 is evolutionarily conserved. Biochemical Biophys Res Commun. 2021;574:48–55.
46. Pal A, Young MA, Donato NJ. Emerging potential of therapeutic targeting of ubiquitin-specific proteases in the treatment of cancer. Cancer Res. 2014;74:4955–66.

ACKNOWLEDGEMENTS

Authors thank Prof. Yang Wang (Dalian Medical University) for generously providing reagents.

AUTHOR CONTRIBUTIONS

HL conceived and designed the project. SW, TW, SC performed experiments and generated figures. XZ and CC carried out bioinformatic analysis. SW, TW, GY, FW, RW and QZ collected the data. SW, TW, DY, YZ, SL, HQ, and QL analyzed and interpreted the data. HL supervised the project and wrote the paper.

FUNDING

This work was supported by the National Natural Science Foundation of China (HL, 82273054) and the LiaoNing Revitalization Talents Program (HL, XLYC1807079).

COMPETING INTERESTS

The authors declare no competing interest.

ETHICS

All procedures followed were in accordance with the ethical standards approved by the Institutional Animal Care and Use Committee at Dalian Medical University.

ADDITIONAL INFORMATION

Supplementary information The online version contains supplementary material available at https://doi.org/10.1038/s41418-023-01176-3.

Correspondence and requests for materials should be addressed to Han Liu.

Reprints and permission information is available at http://www.nature.com/reprints

Publisher's note Springer Nature remains neutral with regard to jurisdictional claims in published maps and institutional affiliations.